Available online at www.sciencedirect.com
SCIENCE DIRECT®
Finite Elements in Analysis and Design 40 (2004) 1333–1359
FINITE ELEMENTS IN ANALYSIS AND DESIGN
www.elsevier.com/locate/finel

Non-conventional non-linear two-node hybrid stress-strain curved beam elements

G.M. Kulikov*, S.V. Plotnikova

Department of Applied Mathematics and Mechanics, Tambov State Technical University, Sovetskaya Street, 106, Tambov 392000, Russia

Received 18 May 2003; accepted 15 September 2003

Abstract

This paper presents a family of two-node hybrid stress–strain curved beam elements with four displacement degrees of freedom (dof) per node for the finite deformation 2D Timoshenko beam theory, which can be readily generalized on the two-node curved beam elements with six displacement dof for the 3D beam theory. The developed formulation is based on the principally new non-linear strain–displacement relationships that are objective, i.e., invariant under arbitrarily large rigid-body motions. To avoid shear and membrane locking and have no spurious zero energy modes, the assumed stress resultant and strain fields are invoked. In order to circumvent thickness locking, the modified material stiffness matrices corresponding to the plane stress state are employed. The fundamental unknowns consist of four displacements and five strains of the face lines of the beam, and five stress resultants. The element characteristic arrays are obtained by using the Hu-Washizu variational principle. To demonstrate the efficiency and accuracy of this formulation and to compare its performance with other non-linear finite element models reported in the literature, extensive numerical studies are presented.

Keywords: Hybrid stress–strain element; Finite deformations; Timoshenko beam; Large rigid-body motions

1. Introduction

Using the solid-shell concept in a non-linear finite element (FE) formulation is well established and has been shown to give acceptable results [1–13]. In order to develop the solid-shell elements that overcome shear, membrane, trapezoidal and thickness locking, advanced FE techniques were

* Corresponding author. Fax: +7-075-271-0216.
E-mail address: kulikov@apmath.tstu.ru (G.M. Kulikov).
URL: http://apm.tstu.ru/kulikov

0168-874X/$ - see front matter © 2003 Elsevier B.V. All rights reserved.
doi:10.1016/j.finel.2003.09.004

applied. In this light, in some works [1,4,5,8–10,12,13] for constructing the solid-shell elements only displacement dof are used. A main idea of such approach is that displacement vectors of the face surfaces of the shell are represented in some global Cartesian basis in order to exactly describe rigid-body motions. Another advantages of the solid-shell formulation compared to the degenerated shell concept [14] are discussed in a review by Sze [15].

Herein, it is developed a close non-linear FE formulation [16–20] based on the Timoshenko beam and Timoshenko–Mindlin-type shell theories with four displacement dof for the 2D beam theory, which can be readily generalized on the 3D beam formulation with six displacement dof. But in our FE development selecting as unknowns the displacements of the face surfaces has a principally another mechanical sense and allows to formulate two-node *curved* beam or four-node curved shell elements with very attractive properties, since objective non-linear strain–displacement relationships, i.e., invariant under large rigid-body motions are applied. Taking into account that here the displacement vectors of the face lines or surfaces are represented in the *local* reference line or surface basis, the developed FE formulation has computational advantages compared to conventional isoparametric FE formulations because it eliminates the costly numerical integration by deriving the stiffness matrix. Indeed, our element matrix requires only direct substitutions (no inversion is needed) and it is evaluated by using the full exact analytical integration.

The proposed theory is free of assumptions of small displacements, small rotations, small strains and small loads because herein the *exact* curved beam theory based on the fully non-linear strain–displacement equations is discussed. There exists only one limitation that a loading step cannot be too large. This restriction arises in a case of using the Newton–Raphson method, since the iteration process can be diverged due to an escape of the initial guess (a result of solving the geometrically linear problem) from Newton's attraction area.

The FE formulation is based on a simple and efficient approximation of beams via two-node curved elements. To avoid shear and membrane locking and have no spurious zero energy modes, the assumed stress resultant and strain fields are invoked. This approach can be treated as a hybrid stress–strain formulation and was proposed by Wempner et al. [21] for the geometrically linear Timoshenko–Mindlin-type shell without the thickness change. In order to circumvent thickness locking, the modified material stiffness matrices symmetric [1,5,9,22] or non-symmetric [19,20,23,24] corresponding to the plane stress state are employed. The fundamental unknowns consist of four displacements and five strains of the face lines of the beam, and five stress resultants. Therefore, for deriving element characteristic arrays the Hu-Washizu variational principle should be applied.

To demonstrate the efficiency and high accuracy of the developed FE formulation and to compare its performance with other approaches reported in the literature, several numerical examples are employed.

2. Strain–displacement equations

Some of the mechanical effects occurring in shells may in principle be discussed with the help of a curved beam. The 2D beam can serve as a model problem to investigate the main difficulties arising when one formulates the finite deformation shell theory with or without thickness change. The advantage is that the mathematical formulation is simpler, since the twisting of the shell is not presented in a 2D beam analysis.

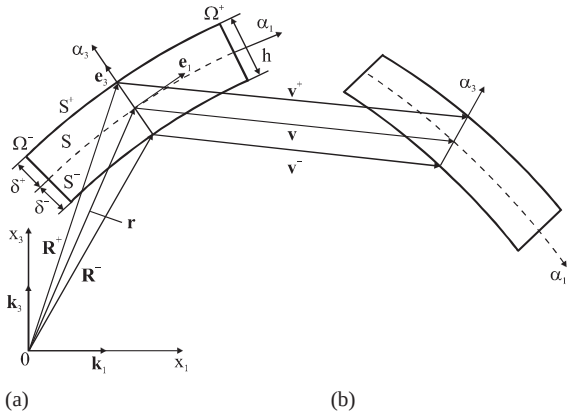

Fig. 1. Curved beam: (a) initial configuration and (b) final configuration.

Let us consider a curved beam of uniform thickness h. The beam may be defined as a 2D body bounded by two bounding lines S^- and S^+, located at distances δ^- and δ^+ measured with respect to the reference line S, and edge boundary lines Ω^- and Ω^+ that are perpendicular to the reference line. For the 2D beam formulation in curvilinear coordinates α_1 denotes the direction of the reference line S and α_3 denotes the transverse direction. The initial configuration of a curved beam is shown in Fig. 1(a) while Fig. 1(b) illustrates the final configuration.

The curvilinear components of the Green–Lagrange strain tensor for finite displacements and strains can be written in a vector form as

$$\varepsilon_{ii}^e = \frac{1}{H_i}\frac{\partial \mathbf{u}}{\partial \alpha_i}\left(\mathbf{e}_i + \frac{1}{2H_i}\frac{\partial \mathbf{u}}{\partial \alpha_i}\right) \quad (i = 1,3), \tag{1a}$$

$$2\varepsilon_{13}^e = \frac{1}{H_1}\frac{\partial \mathbf{u}}{\partial \alpha_1}\left(\mathbf{e}_3 + \frac{1}{2H_3}\frac{\partial \mathbf{u}}{\partial \alpha_3}\right) + \frac{1}{H_3}\frac{\partial \mathbf{u}}{\partial \alpha_3}\left(\mathbf{e}_1 + \frac{1}{2H_1}\frac{\partial \mathbf{u}}{\partial \alpha_1}\right), \tag{1b}$$

$$\mathbf{u} = u_1\mathbf{e}_1 + u_3\mathbf{e}_3, \tag{1c}$$

$$H_1 = A_1(1 + k_1\alpha_3), \quad H_3 = 1, \quad A_1 = \left|\frac{\partial \mathbf{r}}{\partial \alpha_1}\right|, \tag{1d}$$

where $\mathbf{u}$ is the displacement vector; $u_i(\alpha_1, \alpha_3)$ are the components of this vector, which are always measured in accordance with the total Lagrangian formulation from the initial configuration to the final configuration directly (Fig. 1); $\mathbf{e}_1$ and $\mathbf{e}_3$ are the tangent and normal unit vectors to the reference line; r is the position vector of any point of the reference line; A_1 and k_1 are the Lamé parameter and curvature of the reference line. Note that displacement vector (1c) is represented in the local reference line basis $\mathbf{e}_1$ and $\mathbf{e}_3$ that allows one to eliminate the costly numerical integration by deriving the elemental stiffness matrix.

The finite deformation Timoshenko beam theory is based on the linear approximation of displacements in the thickness direction [16,23]:

$$\mathbf{u} = N^-(\alpha_3)\mathbf{v}^- + N^+(\alpha_3)\mathbf{v}^+, \tag{2a}$$

$$\mathbf{v}^{\pm} = v_1^{\pm}\mathbf{e}_1 + v_3^{\pm}\mathbf{e}_3, \tag{2b}$$

$$N^-(\alpha_3) = (\delta^+ - \alpha_3)/h, \quad N^+(\alpha_3) = (\alpha_3 - \delta^-)/h, \tag{2c}$$

where $\mathbf{v}^{\pm}$ are the displacement vectors of the face lines $S^{\pm}$; $v_i^{\pm}(\alpha_1)$ are the displacements of the face lines; $N^{\pm}(\alpha_3)$ are the linear shape functions. The advantage of the proposed approach is apparent, since with the help of displacements $v_i^{\pm}$ the kinematic boundary conditions at the face lines of the beam can be formulated. Moreover, this simplifies a formulation of new FE beam-plate-shell models [17–20] and provides a convenient way to express non-linear strain–displacement relationships in terms of the face line-plane-surface strains.

Substituting displacements (2a) into strain–displacement equations (1) and taking into account formulas for the derivative of the unit vector $\mathbf{e}_3$ along the coordinate line α_1, one can obtain the following strain–displacement equations of the finite deformation Timoshenko theory of *thick* beams:

$$\varepsilon_{11}^a = \left[N^-(\alpha_3)\frac{1}{H_1}\mathbf{v}_{,1}^- + N^+(\alpha_3)\frac{1}{H_1}\mathbf{v}_{,1}^+\right]\mathbf{e}_1 + \frac{1}{2}\left[N^-(\alpha_3)\frac{1}{H_1}\mathbf{v}_{,1}^- + N^+(\alpha_3)\frac{1}{H_1}\mathbf{v}_{,1}^+\right]^2, \tag{3a}$$

$$2\varepsilon_{13}^a = \frac{\bar{H}_1}{H_1}\,6\boldsymbol{\beta}\mathbf{e}_1 + \frac{1}{H_1}\bar{\mathbf{v}}_{,1}(\mathbf{e}_3 + \boldsymbol{\beta}) + (\alpha_3 - \bar{\delta})\frac{1}{H_1}\varepsilon_{33,1}^a, \tag{3b}$$

$$\varepsilon_{33}^a = \boldsymbol{\beta}\left(\mathbf{e}_3 + \tfrac{1}{2}\boldsymbol{\beta}\right), \quad \boldsymbol{\beta} = \frac{1}{h}(\mathbf{v}^+ - \mathbf{v}^-), \quad \bar{\mathbf{v}} = \tfrac{1}{2}(\mathbf{v}^- + \mathbf{v}^+), \tag{3c}$$

$$\bar{H}_1 = A_1(1 + k_1\bar{\delta}),$$

where $\bar{\delta} = (\delta^- + \delta^+)/2$ is the distance from the reference line to the middle line of the beam. Here and in the following developments the abbreviation $()_{,1}$ implies the ordinary derivative with respect to the coordinate α_1.

Replacing further function $H_1 = A_1(1 + k_1\alpha_3)$ correspondingly by its values on the top and bottom lines $H_1^{\pm} = A_1(1 + k_1\delta^{\pm})$ in formula (3a) and by its value on the middle line $\bar{H}_1 = A_1(1 + k_1\bar{\delta})$ in formula (3b), the strain–displacement equations of the finite deformation Timoshenko theory of *moderately thick* beams are obtained:

$$\varepsilon_{11}^b = \left[N^-(\alpha_3)\frac{1}{H_1^-}\mathbf{v}_{,1}^- + N^+(\alpha_3)\frac{1}{H_1^+}\mathbf{v}_{,1}^+\right]\mathbf{e}_1 + \frac{1}{2}\left[N^-(\alpha_3)\frac{1}{H_1^-}\mathbf{v}_{,1}^- + N^+(\alpha_3)\frac{1}{H_1^+}\mathbf{v}_{,1}^+\right]^2, \tag{4a}$$

$$2\varepsilon_{13}^b = \boldsymbol{\beta}\mathbf{e}_1 + \frac{1}{\bar{H}_1}\bar{\mathbf{v}}_{,1}(\mathbf{e}_3 + \boldsymbol{\beta}) + (\alpha_3 - \bar{\delta})\frac{1}{\bar{H}_1}\varepsilon_{33,1}^b, \tag{4b}$$

$$\varepsilon_{33}^b = \boldsymbol{\beta}\left(\mathbf{e}_3 + \tfrac{1}{2}\boldsymbol{\beta}\right), \quad \boldsymbol{\beta} = \frac{1}{h}(\mathbf{v}^+ - \mathbf{v}^-), \quad \bar{\mathbf{v}} = \tfrac{1}{2}(\mathbf{v}^- + \mathbf{v}^+). \tag{4c}$$

The strain–displacement equations (4) are more attractive than (3) because they are completely free for arbitrarily large rigid-body motions. It will be shown in the next section. Note also that longitudinal strain ε_{11}^b is distributed over the beam thickness according to the quadratic law. Taking into account that a beam has a moderate thickness, this complication of the Timoshenko curved

beam theory would be unreasonable because of the minor significance of the quadratic term in most problems.

Therefore, more convenient strain–displacement equations of the refined finite deformation Timoshenko beam theory can be written as

$$\varepsilon_{11}^{c} = N^{-}(\alpha_3)\frac{1}{H_1^{-}}\,\mathbf{v}_{,1}^{-}\left(\mathbf{e}_1 + \frac{1}{2H_1^{-}}\,\mathbf{v}_{,1}^{-}\right) + N^{+}(\alpha_3)\frac{1}{H_1^{+}}\,\mathbf{v}_{,1}^{+}\left(\mathbf{e}_1 + \frac{1}{2H_1^{+}}\,\mathbf{v}_{,1}^{+}\right), \tag{5a}$$

$$2\varepsilon_{13}^{c} = \boldsymbol{\beta}\mathbf{e}_1 + \frac{1}{\bar{H}_1}\,\bar{\mathbf{v}}_{,1}(\mathbf{e}_3 + \boldsymbol{\beta}) + (\alpha_3 - \bar{\delta})\frac{1}{\bar{H}_1}\,\varepsilon_{33,1}^{c}, \tag{5b}$$

$$\varepsilon_{33}^{c} = \boldsymbol{\beta}\left(\mathbf{e}_3 + \tfrac{1}{2}\,\boldsymbol{\beta}\right), \quad \boldsymbol{\beta} = \frac{1}{h}\,(\mathbf{v}^{+} - \mathbf{v}^{-}), \quad \bar{\mathbf{v}} = \tfrac{1}{2}\,(\mathbf{v}^{-} + \mathbf{v}^{+}). \tag{5c}$$

These strain–displacement equations are also completely free for large rigid-body motions.

For the FE implementation of strain–displacement equations (5) they have to be written in a scalar form. Allowing for formulas for the derivatives of the basis vectors [25], one can obtain more convenient equations

$$\varepsilon_{1i}^{c} = N^{-}(\alpha_3)\mathscr{E}_{1i}^{-} + N^{+}(\alpha_3)\mathscr{E}_{1i}^{+}, \quad \varepsilon_{33}^{c} = \mathscr{E}_{33}. \tag{6}$$

Here $\mathscr{E}_{1i}^{\pm}$ are the longitudinal and transverse shear strains of the face lines $S^{\pm}$; $\mathscr{E}_{33}$ is the transverse normal strain defined as

$$\mathscr{E}_{1i}^{\pm} = e_{1i}^{\pm} + \eta_{1i}^{\pm}, \quad \mathscr{E}_{33} = e_{33} + \eta_{33}, \tag{7a}$$

where

$$e_{11}^{\pm} = \frac{1}{\varsigma_1^{\pm}}\,\lambda_1^{\pm}, \quad 2e_{13}^{\pm} = \left(1 \pm \frac{k_1 h}{2\bar{\varsigma}_1}\right)\beta_1 - \frac{1}{\bar{\varsigma}_1}\,\theta_1^{\pm}, \quad e_{33} = \beta_3, \tag{7b}$$

$$\eta_{11}^{\pm} = \frac{1}{2(\varsigma_1^{\pm})^2}[(\lambda_1^{\pm})^2 + (\theta_1^{\pm})^2], \quad 2\eta_{13}^{\pm} = \frac{1}{\bar{\varsigma}_1}(\beta_1\lambda_1^{\pm} - \beta_3\theta_1^{\pm}), \quad \eta_{33} = \tfrac{1}{2}\,(\beta_1^2 + \beta_3^2),$$

$$\lambda_1^{\pm} = \frac{1}{A_1}\,v_{1,1}^{\pm} + k_1 v_3^{\pm}, \quad \theta_1^{\pm} = -\frac{1}{A_1}\,v_{3,1}^{\pm} + k_1 v_1^{\pm},$$

$$\beta_i = \frac{1}{h}\,(v_i^{+} - v_i^{-}), \quad \varsigma_1^{\pm} = 1 + k_1\delta^{\pm}, \quad \bar{\varsigma}_1 = 1 + k_1\bar{\delta}.$$

Remark 2.1. The components of Green–Lagrange strain tensors (3)–(5) satisfy the first type of coupling conditions

$$\varepsilon_{11}^{a}(\delta^{\pm}) = \varepsilon_{11}^{b}(\delta^{\pm}) = \varepsilon_{11}^{c}(\delta^{\pm}) = \mathscr{E}_{11}^{\pm},$$

$$\varepsilon_{13}^{a}(\bar{\delta}) = \varepsilon_{13}^{b}(\bar{\delta}) = \varepsilon_{13}^{c}(\bar{\delta}) = \bar{\mathscr{E}}_{13}.$$

This is illustrated in Fig. 2, where $\bar{\mathscr{E}}_{13} = (\mathscr{E}_{13}^{-} + \mathscr{E}_{13}^{+})/2$ is the transverse shear strain of the middle line.

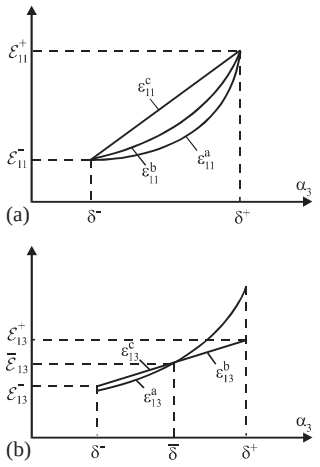

Fig. 2. Distribution of (a) longitudinal strain and (b) transverse shear strain over beam thickness.

Remark 2.2. The components of the Green–Lagrange strain tensor (4) as will as the strain tensor (5) satisfy the second type of coupling conditions

$$2[\varepsilon_{13}^{b}(\delta^{+}) - \varepsilon_{13}^{b}(\delta^{-})] = \frac{1}{\bar{H}_1} h\varepsilon_{33,1}^{b}, \tag{8a}$$

$$2[\varepsilon_{13}^{c}(\delta^{+}) - \varepsilon_{13}^{c}(\delta^{-})] = \frac{1}{\bar{H}_1} h\varepsilon_{33,1}^{c}, \tag{8b}$$

which immediately follows from relationships (4) and (5). Allowing for notation (7a), one can write

$$2(\mathscr{E}_{13}^{+} - \mathscr{E}_{13}^{-}) = \frac{1}{\bar{H}_1} h\mathscr{E}_{33,1}. \tag{8c}$$

Coupling condition (8c) plays a central role in our FE formulation (see Section 6).

Finally, consider a limit case when the transverse shear strain is independent on the thickness coordinate. This case corresponds to the classical Timoshenko curved beam theory without the thickness change and is important for the FE implementation. In a result we have the following strain–displacement equations:

$$\varepsilon_{11}^{d} = N^{-}(\alpha_3)\frac{1}{H_1^{-}}\mathbf{v}_{,1}^{-}\left(\mathbf{e}_1 + \frac{1}{2H_1^{-}}\mathbf{v}_{,1}^{-}\right) + N^{+}(\alpha_3)\frac{1}{H_1^{+}}\mathbf{v}_{,1}^{+}\left(\mathbf{e}_1 + \frac{1}{2H_1^{+}}\mathbf{v}_{,1}^{+}\right), \tag{9a}$$

$$2\varepsilon_{13}^{d} = \boldsymbol{\beta}\mathbf{e}_1 + \frac{1}{\bar{H}_1}\bar{\mathbf{v}}_{,1}(\mathbf{e}_3 + \boldsymbol{\beta}), \tag{9b}$$

$$\varepsilon_{33}^{d} = \boldsymbol{\beta}\left(\mathbf{e}_3 + \tfrac{1}{2}\boldsymbol{\beta}\right), \quad \boldsymbol{\beta} = \frac{1}{h}(\mathbf{v}^{+} - \mathbf{v}^{-}), \quad \bar{\mathbf{v}} = \tfrac{1}{2}(\mathbf{v}^{-} + \mathbf{v}^{+}). \tag{9c}$$

3. Large rigid-body motions

An arbitrarily large rigid-body motion can be defined as

$$\mathbf{u}^R = \mathbf{\Delta} + (\mathbf{\Phi} - \mathbf{E})\mathbf{R}, \tag{10}$$

where $\mathbf{R} = \mathbf{r} + \alpha_3\mathbf{e}_3$ is the position vector of any point of the beam; $\mathbf{\Delta} = \Delta_1\mathbf{e}_1 + \Delta_3\mathbf{e}_3$ is the constant displacement (translation) vector; $\mathbf{E}$ is the identity matrix; $\mathbf{\Phi}$ is the orthogonal matrix; we also refer to $\mathbf{\Phi}$ as a rotation matrix.

In particular, rigid-body motions of the face lines are

$$\mathbf{v}^{\pm R} = \mathbf{\Delta} + (\mathbf{\Phi} - \mathbf{E})\mathbf{R}^{\pm}, \tag{11}$$

where $\mathbf{R}^{\pm} = \mathbf{r} + \delta^{\pm}\mathbf{e}_3$ are the position vectors of points of the top and bottom lines $S^{\pm}$ (Fig. 1).

The derivatives of the translation and position vectors, and unit vector of the reference line with respect to the coordinate α_1 can be written as

$$\mathbf{\Delta}_{,1} = \mathbf{0}, \quad \mathbf{r}_{,1} = A_1\mathbf{e}_1, \quad \mathbf{e}_{3,1} = A_1k_1\mathbf{e}_1. \tag{12}$$

Taking into account formulas (11) and (12), one can obtain the following expression for the derivative:

$$\mathbf{v}_{,1}^{\pm R} = H_1^{\pm}(\mathbf{\Phi}\mathbf{e}_1 - \mathbf{e}_1). \tag{13}$$

It can be shown by using formulas (11) and (13) that strains from Eqs. (4) and (5) are all zero in a general large rigid-body motion, i.e.,

$$\varepsilon_{ii}^{bR} = \tfrac{1}{2}[(\mathbf{\Phi}\mathbf{e}_i)(\mathbf{\Phi}\mathbf{e}_i) - \mathbf{e}_i\mathbf{e}_i] = 0,$$

$$\varepsilon_{13}^{bR} = \tfrac{1}{2}[(\mathbf{\Phi}\mathbf{e}_1)(\mathbf{\Phi}\mathbf{e}_3) - \mathbf{e}_1\mathbf{e}_3] + (\alpha_3 - \bar{\delta})\frac{1}{2\bar{H}_1}\varepsilon_{33,1}^{bR} = 0. \tag{14}$$

This conclusion is true because an orthogonal transformation retains the scalar product of the vectors. To write the remaining equations, we should replace in Eq. (14) superscript b by c. So, strain–displacement relationships (4) and (5) are invariant under arbitrarily large rigid-body motions.

One can verify applying formulas (11) and (13) that strain–displacement relationships (9) are also invariant under large rigid-body motions because

$$\varepsilon_{ij}^{dR} = \tfrac{1}{2}[(\mathbf{\Phi}\mathbf{e}_i)(\mathbf{\Phi}\mathbf{e}_j) - \mathbf{e}_i\mathbf{e}_j] = 0 \quad (i, j = 1, 3). \tag{15}$$

It should be noted that using a similar technique the more general finite deformation layer-wise Timoshenko beam theory can be developed. This theory is under development and will be published in next papers.

4. Stress–strain equations

In this section three types of the constitutive equations are discussed.

4.1. Complete constitutive equations

Consider an orthotropic layer of the beam whose axes of symmetry coincide with coordinate directions α_1 and α_3. In this case the equations of the complete 2D Hooke's law will be

$$\varepsilon_{11} = \frac{1}{E_1} S_{11} - \frac{\nu_{31}}{E_3} S_{33}, \tag{16a}$$

$$\varepsilon_{33} = -\frac{\nu_{13}}{E_1} S_{11} + \frac{1}{E_3} S_{33}, \tag{16b}$$

$$2\varepsilon_{13} = \frac{1}{G_{13}} S_{13}, \tag{16c}$$

where S_{ij} are the components of the second Piola–Kirchhoff stress tensor, E_1 and E_2 are the elastic moduli, G_{13} is the shear modulus, ν_{13} and ν_{31} are Poisson's ratios.

Solving Eq. (16) for the stresses, one can find

$$\begin{bmatrix} S_{11} \\ S_{33} \\ S_{13} \end{bmatrix} = \begin{bmatrix} C_{1111} & C_{1133} & 0 \\ C_{3311} & C_{3333} & 0 \\ 0 & 0 & C_{1313} \end{bmatrix} \begin{bmatrix} \varepsilon_{11} \\ \varepsilon_{33} \\ 2\varepsilon_{13} \end{bmatrix}, \tag{17a}$$

where

$$C_{1111} = \frac{E_1}{1-\nu_{13}\nu_{31}}, \quad C_{3333} = \frac{E_3}{1-\nu_{13}\nu_{31}}, \tag{17b}$$

$$C_{1133} = \frac{\nu_{31}E_1}{1-\nu_{13}\nu_{31}}, \quad C_{3311} = \frac{\nu_{13}E_3}{1-\nu_{13}\nu_{31}}, \quad C_{1313} = G_{13}.$$

Unfortunately, such a formulation on the basis of the complete 2D constitutive law is deficient because thickness locking [15] can occur. This phenomenon occurs in bending dominated beam problems when Poisson's ratio is not equal to zero. The reason is that Poisson's effect in the thickness direction is taken into account in Eq. (16a) of Hooke's law. Therefore, Poisson's ratio ν_{31} should be formally set to zero.

4.2. Reduced constitutive equations

In order to avoid thickness locking, we invoke the standard engineering assumption

$$S_{33} \ll S_{11}. \tag{18}$$

Allowing for assumption (18) into Eq. (16a), one obtains

$$S_{11} = E_1\varepsilon_{11}. \tag{19}$$

Substituting further longitudinal stress (19) into Eq. (16b) and solving for the transverse normal stress, we arrive at the following equation:

$$S_{33} = E_3(\nu_{13}\varepsilon_{11} + \varepsilon_{33}). \tag{20}$$

Now, we can write reduced stress–strain equations of the 2D constitutive law in a matrix form (17a), where material moduli will be

$$C_{1111} = E_1, \quad C_{3333} = E_3, \quad C_{1133} = 0, \quad C_{3311} = \nu_{13}E_3, \quad C_{1313} = G_{13}. \tag{21}$$

Comparing Eqs. (17b) and (21) one may observe that these equations are exactly the same when Poisson's ratio $\nu_{31} = 0$. This partially substantiates our modification of the complete 2D constitutive law.

The described approach was developed by Kulikov and Plotnikova [19,20,23,24] for overcoming simultaneously thickness and volumetric locking. It should be mentioned that this approach lead to the non-symmetric material stiffness matrices and as a result more computational efforts have to be made.

4.3. Simplified constitutive equations based on the plane stress conditions

When a beam is under pure bending, the transverse normal stress is zero. So, the simplified material stiffness matrix can be employed

$$C_{1111} = E_1, \quad C_{3333} = E_3, \quad C_{1133} = C_{3311} = 0, \quad C_{1313} = G_{13}. \tag{22}$$

This is due to the plane stress enforcement which is done by decoupling the transverse normal stress with all other stresses in the complete 3D Hooke's law [1,5,9,22] and in particular with the longitudinal stress in the 2D Hooke's law (16).

A comparison of Eqs. (21) and (22) shows that corresponding equations are identical for the zero Poisson's ratio ν_{13}.

5. Hu-Washizu variational equation for multilayered composite beam

Let us consider the curved beam built up in the general case by the arbitrary superposition across the thickness of N layers of uniform thickness h_k. The kth layer may be defined as a 2D body bounded by two lines S_{k-1} and S_k, located at the distances δ_{k-1} and δ_k measured with respect to the reference line S, and the edge boundary lines $\Omega_k^{\pm}$ that are perpendicular to the reference line (Fig. 3). It is also assumed that the bounding lines S_{k-1} and S_k are continuous and sufficiently smooth. Let the reference line be referred to the curvilinear coordinate system α_1. The α_3 axis is oriented along the outward unit vector $\mathbf{e}_3$ normal to the reference line.

The constituent layers of the beam are supposed to be rigidly joined, so that no slip on contact lines and no separation of layers can occur. The material of each constituent layer is assumed to be linearly elastic and orthotropic. Let p_i^- and p_i^+ be the intensities of the external loading acting on the bottom line $S^- = S_0$ and top line $S^+ = S_N$ in the α_i coordinate directions, respectively; $\overset{\vee}{\mathbf{q}}{}^{(k)}$ and $\hat{\mathbf{q}}^{(k)}$ be the external loading vectors acting on the edge boundary lines Ω_k^- and Ω_k^+, where $\Omega_k^{\pm} = \{(\alpha_1, \alpha_3) | \alpha_1 = \alpha_1^{\pm}, \alpha_3 \in [\delta_{k-1}, \delta_k]\}$. Here and in the following developments the index k identifies the belonging of any quantity to the kth layer ($k = \overline{1,N}$), and indices i, j, ℓ, m take the values 1 and 3.

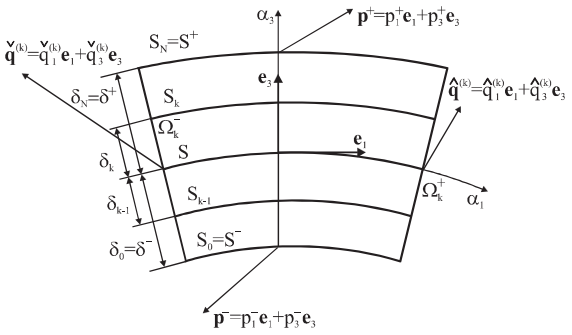

Fig. 3. Multilayered curved beam.

The Hu-Washizu variational principle [26] for the 2D multilayered beam can be written in the following form:

$$\int_S \sum_{i,j}\sum_k \int_{\delta_{k-1}}^{\delta_k} [(S_{ij}^{(k)} - \sum_{\ell,m} C_{ij\ell m}^{(k)}\varepsilon_{\ell m})\delta\varepsilon_{ij} + (\varepsilon_{ij} - \varepsilon_{ij}^u)\delta S_{ij}^{(k)} - S_{ij}^{(k)}\delta\varepsilon_{ij}^u]H_1\,\mathrm{d}\alpha_3\,\mathrm{d}\alpha_1$$
$$+ \int_{S^+}\sum_i p_i^+\delta u_i H_1^+\,\mathrm{d}\alpha_1 - \int_{S^-}\sum_i p_i^-\delta u_i H_1^-\,\mathrm{d}\alpha_1$$
$$+ \sum_i\sum_k \left(\int_{\Omega_k^+} \hat{q}_i^{(k)}\,\delta u_i\,\mathrm{d}\alpha_3 - \int_{\Omega_k^-} \overset{\vee}{q}{}_i^{(k)}\,\delta u_i\,\mathrm{d}\alpha_3\right) = 0, \tag{23}$$

where ε_{ij}^u are the strains due to the displacement field; ε_{ij} are the independently assumed strains; $S_{ij}^{(k)}$ are the components of the second Piola–Kirchhoff stress tensor of the kth layer; $C_{ij\ell m}^{(k)}$ are the material moduli of the kth layer.

The finite deformation multilayered Timoshenko beam theory is based on the approximations of displacements in the thickness direction (2), where we should set $\delta^- = \delta_0$ and $\delta^+ = \delta_N$, and displacement-dependent and assumed displacement-independent strains

$$\varepsilon_{1i}^u = \varepsilon_{1i}^c = N^-(\alpha_3)\mathscr{E}_{1i}^- + N^+(\alpha_3)\mathscr{E}_{1i}^+, \quad \varepsilon_{33}^u = \varepsilon_{33}^c = \mathscr{E}_{33}, \tag{24a}$$

$$\varepsilon_{1i} = N^-(\alpha_3)E_{1i}^- + N^+(\alpha_3)E_{1i}^+, \quad \varepsilon_{33} = E_{33}. \tag{24b}$$

Substituting approximations (2) and (24) into variational equation (23), and allowing for that metrics of all lines parallel to the reference line are identical and equal to the metric of the middle line $\bar{S}$, one can find

$$\int_{\bar{S}} [(\mathbf{T} - \mathbf{D}\mathbf{E})^t\delta\mathbf{E} + (\mathbf{E} - \mathscr{E})^t\delta\mathbf{T} - \mathbf{T}^t\delta\mathscr{E} + \mathbf{P}^t\delta\mathbf{v}]\bar{H}_1\,\mathrm{d}\alpha_1 + \hat{\mathbf{T}}^t\delta\hat{\mathbf{v}} - \overset{\vee}{\mathbf{T}}{}^t\delta\overset{\vee}{\mathbf{v}} = 0. \tag{25}$$

Here matrix notations are introduced

$$\mathbf{v} = [v_1^-\ v_1^+\ v_3^-\ v_3^+]^t, \quad \mathbf{P} = [-p_1^-\ p_1^+ - p_3^-\ p_3^+]^t, \tag{26}$$

$$\boldsymbol{\mathscr{E}} = [\mathscr{E}_{11}^{-}\ \mathscr{E}_{11}^{+}\ 2\mathscr{E}_{13}^{-}\ 2\mathscr{E}_{13}^{+}\ \mathscr{E}_{33}]^t, \quad \mathbf{E} = [E_{11}^{-}\ E_{11}^{+}\ 2E_{13}^{-}\ 2E_{13}^{+}\ E_{33}]^t,$$

$$\mathbf{T} = [T_{11}^{-}\ T_{11}^{+}\ T_{13}^{-}\ T_{13}^{+}\ T_{33}]^t, \quad \hat{\mathbf{T}} = [\hat{T}_{11}^{-}\ \hat{T}_{11}^{+}\ \hat{T}_{13}^{-}\ \hat{T}_{13}^{+}]^t, \quad \breve{\mathbf{T}} = [\breve{T}_{11}^{-}\ \breve{T}_{11}^{+}\ \breve{T}_{13}^{-}\ \breve{T}_{13}^{+}]^t,$$

$$\hat{\mathbf{v}} = [v_1^{-}(\alpha_1^{+})\ v_1^{+}(\alpha_1^{+})\ v_3^{-}(\alpha_1^{+})\ v_3^{+}(\alpha_1^{+})]^t, \quad \breve{\mathbf{v}} = [v_1^{-}(\alpha_1^{-})\ v_1^{+}(\alpha_1^{-})\ v_3^{-}(\alpha_1^{-})\ v_3^{+}(\alpha_1^{-})]^t,$$

$$\mathbf{D} = \begin{bmatrix} D_{1111}^{00} & D_{1111}^{01} & 0 & 0 & D_{1133}^{-} \\ D_{1111}^{01} & D_{1111}^{11} & 0 & 0 & D_{1133}^{+} \\ 0 & 0 & D_{1313}^{00} & D_{1313}^{01} & 0 \\ 0 & 0 & D_{1313}^{01} & D_{1313}^{11} & 0 \\ D_{3311}^{-} & D_{3311}^{+} & 0 & 0 & D_{3333} \end{bmatrix},$$

where $T_{1i}^{\pm}$ and T_{33} are the stress resultants; $\hat{T}_{1i}^{\pm}$ and $\breve{T}_{1i}^{\pm}$ are the external load resultants; D_{1i1i}^{pq}, $D_{iijj}^{\pm}$ and D_{3333} are the components of the through-the-thickness stiffness matrix, which are defined as

$$T_{1i}^{\pm} = \sum_k \int_{\delta_{k-1}}^{\delta_k} S_{1i}^{(k)} N^{\pm}(\alpha_3)\,\mathrm{d}\alpha_3, \quad T_{33} = \sum_k \int_{\delta_{k-1}}^{\delta_k} S_{33}^{(k)}\,\mathrm{d}\alpha_3, \tag{27a}$$

$$\hat{T}_{1i}^{\pm} = \sum_k \int_{\delta_{k-1}}^{\delta_k} \hat{q}_i^{(k)} N^{\pm}(\alpha_3)\,\mathrm{d}\alpha_3, \quad \breve{T}_{1i}^{\pm} = \sum_k \int_{\delta_{k-1}}^{\delta_k} \breve{q}_i^{(k)} N^{\pm}(\alpha_3)\,\mathrm{d}\alpha_3, \tag{27b}$$

$$D_{1i1i}^{pq} = \sum_k \int_{\delta_{k-1}}^{\delta_k} C_{1i1i}^{(k)} [N^{-}(\alpha_3)]^{2-p-q} [N^{+}(\alpha_3)]^{p+q}\,\mathrm{d}\alpha_3 \quad (p,q=0,1), \tag{27c}$$

$$D_{iijj}^{\pm} = \sum_k \int_{\delta_{k-1}}^{\delta_k} C_{iijj}^{(k)} N^{\pm}(\alpha_3)\,\mathrm{d}\alpha_3 \quad (i \neq j), \quad D_{3333} = \sum_k \int_{\delta_{k-1}}^{\delta_k} C_{3333}^{(k)}\,\mathrm{d}\alpha_3.$$

Variational equation (25) provides a foundation for the FE formulation for multilayered beams undergoing finite rotations on the basis of aforementioned constitutive laws, namely, complete (17), reduced when in accordance with Eq. (21) $D_{1133}^{\pm} = 0$, and simplified when additionally $D_{3311}^{\pm} = 0$, i.e., a plane stress condition is invoked.

6. FE formulation

Variational equation (25) for the beam element can be written in the more convenient form

$$\int_{-1}^{1} [\delta\mathbf{E}^t(\mathbf{T} - \mathbf{D}\mathbf{E}) + \delta\mathbf{T}^t(\mathbf{E} - \boldsymbol{\mathscr{E}}) - \delta\boldsymbol{\mathscr{E}}^t\mathbf{T} + \delta\mathbf{v}^t\mathbf{P}]\bar{H}_1\ell_1^{e\ell}\,\mathrm{d}\xi_1 + \delta\hat{\mathbf{v}}^t\,\hat{\mathbf{T}} - \delta\breve{\mathbf{v}}^t\,\breve{\mathbf{T}} = 0, \tag{28}$$

where $\xi_1 = (\alpha_1 - d_1^{e\ell})/\ell_1^{e\ell}$ is the local curvilinear normalized coordinate (Fig. 4); $d_1^{e\ell} = (\alpha_1^{-e\ell} + \alpha_1^{+e\ell})/2$ is the coordinate of the center of the element; $2\ell_1^{e\ell} = \alpha_1^{+e\ell} - \alpha_1^{-e\ell}$ is the length of the element.

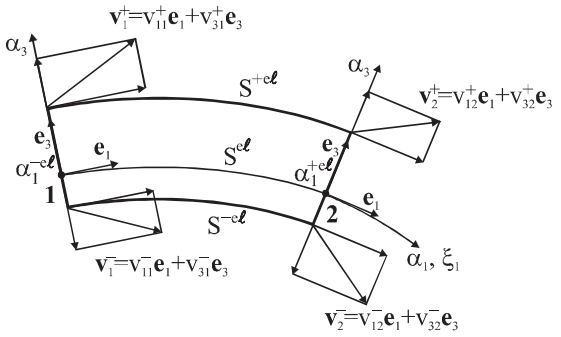

Fig. 4. Two-node curved beam element.

For the simplest two-node beam element the displacement field is approximated according to the standard C^0 interpolation

$$\mathbf{v} = N_1(\xi_1)\mathbf{v}_1 + N_2(\xi_1)\mathbf{v}_2, \tag{29}$$

where $N_r(\xi_1)$ are the linear shape functions of the element; $\mathbf{v}_r = [v_{1r}^- v_{1r}^+ v_{3r}^- v_{3r}^+]^t$ are the displacement vectors of the element nodes; the index r denotes a number of nodes and equals 1 and 2. The load vector is also assumed to vary linearly inside the element.

In a result for the displacement-dependent strains (7) we have the following approximation:

$$\boldsymbol{\mathscr{E}} = \boldsymbol{\mathscr{E}}^0 + \xi_1\boldsymbol{\mathscr{E}}^1 + \xi_1^2\boldsymbol{\mathscr{E}}^2, \tag{30a}$$

$$\boldsymbol{\mathscr{E}}^0 = (\mathbf{B}^0 + \mathbf{J}^0\mathbf{V})\mathbf{V}, \quad \boldsymbol{\mathscr{E}}^1 = (\mathbf{B}^1 + \mathbf{J}^1\mathbf{V})\mathbf{V}, \quad \boldsymbol{\mathscr{E}}^2 = (\mathbf{J}^2\mathbf{V})\mathbf{V}, \tag{30b}$$

$$\boldsymbol{\mathscr{E}}^s = [\mathscr{E}_{11}^{-s}\ \mathscr{E}_{11}^{+s}\ 2\mathscr{E}_{13}^{-s}\ 2\mathscr{E}_{13}^{+s}\ \mathscr{E}_{33}^{s}]^t, \quad \mathbf{V} = [\mathbf{v}_1^t\ \mathbf{v}_2^t]^t, \tag{30c}$$

where $\mathbf{V}$ is the displacement vector at nodal points of the element; $\mathbf{B}^0$ and $\mathbf{B}^1$ are the matrices of order 5×8, corresponding to the linear strain–displacement transformation; $\mathbf{J}^s$ are the 3D arrays of order $5 \times 8 \times 8$, corresponding to the non-linear strain–displacement transformation; $s = \overline{0,2}$. It is apparent that in Eq. (30b) $\mathbf{J}^s\mathbf{V}$ imply matrices of order 5×8 and the following rule is used in calculations:

$$(\mathbf{J}^s\mathbf{V})_{np} = \sum_q \mathbf{J}_{npq}^s\mathbf{V}_q \quad (s = \overline{0,2}; n = \overline{1,5}; p,q = \overline{1,8}).$$

To avoid shear and membrane locking and have no spurious zero energy modes, the assumed stress resultant and strain fields inside the element are introduced

$$E_{1i}^{\pm} = E_{1i}^{\pm 0}, \quad E_{33} = E_{33}^0 + \xi_1 E_{33}^1, \tag{31a}$$

$$T_{1i}^{\pm} = T_{1i}^{\pm 0}, \quad T_{33} = T_{33}^0 + \xi_1 T_{33}^1. \tag{31b}$$

These interpolations can be written in a matrix form as

$$\mathbf{E} = \mathbf{E}^0 + \xi_1 E_{33}^1\mathbf{Q}, \quad \mathbf{T} = \mathbf{T}^0 + \xi_1 T_{33}^1\mathbf{Q}, \tag{32}$$

$$\mathbf{E}^0 = [E_{11}^{-0}\ E_{11}^{+0}\ 2E_{13}^{-0}\ 2E_{13}^{+0}\ E_{33}^{0}]^t, \quad \mathbf{T}^0 = [T_{11}^{-0}\ T_{11}^{+0}\ T_{13}^{-0}\ T_{13}^{+0}\ T_{33}^{0}]^t,$$

$$\mathbf{Q} = [0\ 0\ 0\ 0\ 1]^t.$$

Note that this approach may be treated as a hybrid stress–strain formulation and was proposed by Wempner et al. [21] for the geometrically linear Timoshenko-Mindlin-type shell without the thickness change.

Substituting Eqs. (29)–(32) into variational equation (28) and using the standard variational procedure, one obtains governing equations of the developed FE formulation

$$\mathbf{T}^0 = \mathbf{D}\mathbf{E}^0, \quad T_{33}^1 = D_{3333}E_{33}^1, \tag{33a}$$

$$\mathbf{E}^0 = (\mathbf{B}^0 + \mathbf{A}^0\mathbf{V})\mathbf{V}, \quad E_{33}^1 = \mathbf{Q}^t(\mathbf{B}^1 + \mathbf{A}^1\mathbf{V})\mathbf{V}, \tag{33b}$$

$$(\mathbf{B}^0 + 2\mathbf{A}^0\mathbf{V})^t\mathbf{T}^0 + \tfrac{1}{3}(\mathbf{B}^1 + 2\mathbf{A}^1\mathbf{V})^t\mathbf{Q}T_{33}^1 = \mathbf{F}, \tag{33c}$$

where $\mathbf{F}$ is the force vector; $\mathbf{A}^0$ and $\mathbf{A}^1$ are the 3D arrays of order $5 \times 8 \times 8$ defined as

$$\mathbf{A}^0 = \mathbf{J}^0 + \underline{\tfrac{1}{3}}\,\mathbf{J}^2, \quad \mathbf{A}^1 = \mathbf{J}^1. \tag{33d}$$

Remark 6.1. There exists a link between displacement-independent and displacement-dependent strains

$$\mathbf{E}^0 = \boldsymbol{\mathscr{E}}^0 + \underline{\tfrac{1}{3}}\,\boldsymbol{\mathscr{E}}^2, \quad E_{33}^1 = \mathscr{E}_{33}^1 \tag{34}$$

that immediately follows from Eqs. (30b), (33b) and (33d).

Next, we prove a fundamental result concerning the relation between transverse components of the assumed strain tensor.

Proposition 6.1. The transverse shear and normal displacement-independent strains satisfy the following coupling condition:

$$hE_{33}^1 = 2\bar{H}_1(E_{13}^{+0} - E_{13}^{-0}). \tag{35}$$

Proof. Using Eq. (30a) into Eq. (8c) yields

$$2(\mathscr{E}_{13}^{+0} - \mathscr{E}_{13}^{-0}) + 2\xi_1(\mathscr{E}_{13}^{+1} - \mathscr{E}_{13}^{-1}) + 2\xi_1^2(\mathscr{E}_{13}^{+2} - \mathscr{E}_{13}^{-2}) = \frac{1}{\bar{H}_1}h(\mathscr{E}_{33}^1 + 2\xi_1\mathscr{E}_{33}^2). \tag{36}$$

Accounting for that Eq. (36) is fulfilled for every $\xi_1 \in [-1, 1]$, the following equations are valid:

$$2(\mathscr{E}_{13}^{+0} - \mathscr{E}_{13}^{-0}) = \frac{1}{\bar{H}_1}h\mathscr{E}_{33}^1, \quad \mathscr{E}_{13}^{+1} - \mathscr{E}_{13}^{-1} = \frac{1}{\bar{H}_1}h\mathscr{E}_{33}^2, \quad \mathscr{E}_{13}^{+2} - \mathscr{E}_{13}^{-2} = 0. \tag{37}$$

Eq. (34) can be written in a scalar form as

$$E_{13}^{+0} - E_{13}^{-0} = \mathscr{E}_{13}^{+0} - \mathscr{E}_{13}^{-0} + \tfrac{1}{3}(\mathscr{E}_{13}^{+2} - \mathscr{E}_{13}^{-2}), \quad E_{33}^1 = \mathscr{E}_{13}^1. \tag{38}$$

Finally, from Eqs. (37) and (38) one derives required relation (35).

Coupling Eq. (35) plays an important role in our FE formulation because it implies that only five assumed strain modes are *independent* of six modes from approximation (31a). This provides

a correct rank of the elemental matrix [27], since eight displacement dof are introduced. It should be mentioned that our elemental stiffness matrix requires only direct substitutions (no inversion is needed as we shall see later) and it is evaluated by using the full exact *analytical* integration. So, our FE formulation for curved beams is very economical and efficient compared with the conventional isoparametric FE formulations because it eliminates the costly numerical integration by deriving the stiffness matrices.

Remark 6.2. During the analytical integration it is supposed that geometrical characteristics of the element reference line A_1 and k_1 may be evaluated at the center of the element at $\xi_1 = 0$.

Remark 6.3. The underlined multipliers into Eqs. (33d) and (34) are parasitic and should be dropped, i.e.,

$$\mathbf{A}^0 = \mathbf{J}^0 + \mathbf{J}^2, \quad \mathbf{A}^1 = \mathbf{J}^1, \tag{39a}$$

$$\mathbf{E}^0 = \boldsymbol{\mathscr{E}}^0 + \boldsymbol{\mathscr{E}}^2, \quad E^1_{33} = \mathscr{E}^1_{33}. \tag{39b}$$

The existence of these multipliers makes the non-linear two-node element a bit stiff and some stabilization procedure needs to be applied. The best solution of the problem is to use the assumed natural strain (ANS) method developed by many scientists for the linear and non-linear displacement, mixed and hybrid FE formulations [4,6–8,10,13,28–30].

So, to avoid locking, *non-linear* displacement-dependent strains are assumed to vary linearly inside the element

$$\boldsymbol{\mathscr{E}}^{\mathrm{ANS}} = \tfrac{1}{2}(1-\xi_1)\boldsymbol{\mathscr{E}}(-1) + \tfrac{1}{2}(1+\xi_1)\boldsymbol{\mathscr{E}}(1) \tag{40a}$$

that may be written in accordance with Eq. (30a) in the more convenient form

$$\boldsymbol{\mathscr{E}}^{\mathrm{ANS}} = \boldsymbol{\mathscr{E}}^0 + \boldsymbol{\mathscr{E}}^2 + \xi_1\boldsymbol{\mathscr{E}}^1. \tag{40b}$$

Substituting Eqs. (29), (32) and (40b) into variational equation (28) and allowing for Eq. (30b), one derives governing Eqs. (33a)–(33c) and (39a) instead of Eqs. (33a)–(33d), which were obtained without using the ANS method.

Eliminating further assumed strains and stress resultants from Eqs. (33a)–(33c), the following equilibrium equations are derived:

$$\mathbf{G}(\mathbf{V}) = \mathbf{F}, \tag{41a}$$

where

$$\mathbf{G}(\mathbf{V}) = (\mathbf{B}^0 + 2\mathbf{A}^0\mathbf{V})^t\mathbf{D}(\mathbf{B}^0 + \mathbf{A}^0\mathbf{V})\mathbf{V} + \tfrac{1}{3}(\mathbf{B}^1 + 2\mathbf{A}^1\mathbf{V})^t\mathbf{Q}D_{3333}\mathbf{Q}^t(\mathbf{B}^1 + \mathbf{A}^1\mathbf{V})\mathbf{V}. \tag{41b}$$

Due to the existence of non-linear terms in Eqs. (41), the Newton–Raphson iteration process should be employed to solve these equations

$$\mathbf{V}^{[n+1]} = \mathbf{V}^{[n]} + \left[\frac{\partial \mathbf{G}}{\partial \mathbf{V}}(\mathbf{V}^{[n]})\right]^{-1}[\mathbf{F} - \mathbf{G}(\mathbf{V}^{[n]})], \tag{42}$$

where the superscript n indicates a number of iterations.

The equilibrium equations (42) for each element are assembled by the usual technique to form the global equilibrium equations. These equations should be performed until the required accuracy of the solution can be obtained. The convergence criterion used herein can be described as

$$\|\mathbf{U}^{[n+1]} - \mathbf{U}^{[n]}\| < \varepsilon \|\mathbf{U}^{[n]}\|, \tag{43}$$

where $\|_\bullet\|$ stands for the Euclidean norm in the displacement space; $\mathbf{U}$ is the global vector of displacements; ε is the prescribed tolerance.

7. Numerical tests

The performance of the proposed beam elements is evaluated with several discriminating problems extracted from the literature. A listing of these elements and the abbreviations used to identify them are contained in Table 1.

7.1. Linear 2D beam examples

In order to test the ability of the developed two-node curved beam elements to overcome shear and membrane locking, we consider a standard geometrically linear example.

7.1.1. Pinched circular ring

A circular ring subjected to two opposite concentrated forces was studied by many investigators, e.g. Refs. [31,32]. The geometrical and material properties of the ring are depicted in Fig. 5, where R is the radius of the middle circle.

Owing to symmetry of the problem, only one quarter of the ring is modeled with regular meshes of TB2C, TB2R and TB2S elements. Table 2 lists the radial displacement $\bar{v}_3 = (v_3^- + v_3^+)/2$ normalized to the analytical solution [31]. The results reported by Cho and Lee [32] by using different meshes of nine-node hybrid strain elements are also displayed. It is seen that the developed elements perform well but the TB2C element is too stiff because thickness locking occurs. It is worth noting that all our elemental stiffness matrices have three, and only three, zero eigenvalues as required for satisfaction of the general rigid-body motion representation.

Table 1
Listing of two-node curved beam elements

Name	Description
TB2C	Element[a] based on the complete constitutive law (17a) and (17b)
TB2R	Element[a] based on the reduced constitutive law (17a) and (21)
TB2S	Element[a] based on the simplified constitutive law (17a) and (22)
TB2CA	TB2C element with the ANS interpolation[b]
TB2RA	TB2R element with the ANS interpolation[b]
TB2SA	TB2S element with the ANS interpolation[b]

[a]Identical elements for zero Poisson's ratios.
[b]Identical elements for zero Poisson's ratios.

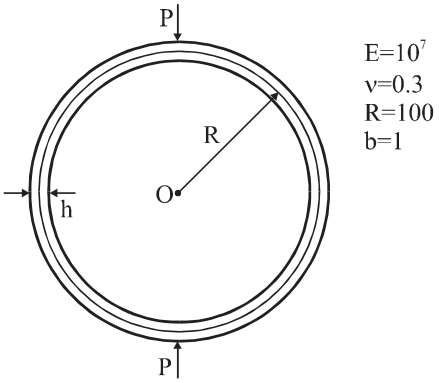

Fig. 5. Pinched circular ring.

Table 2
Radial displacement at loading point of pinched ring normalized to analytical solution $w_{\text{exact}} = 0.8927PR^3/(Eh^3)$ [31]

Element	$R/h = 100$		$R/h = 500$		$R/h = 1000$	
	$N^{el} = 8$	$N^{el} = 16$	$N^{el} = 8$	$N^{el} = 16$	$N^{el} = 8$	$N^{el} = 16$
TB2C	0.8797	0.9024	0.8795	0.9023	0.8797	0.9023
TB2R	0.9667	0.9916	0.9666	0.9915	0.9665	0.9915
TB2S	0.9667	0.9916	0.9666	0.9915	0.9668	0.9915
Cho and Lee [32][a]	0.9983	0.9998	0.9981	0.9996	0.9981	0.9995

[a] 4×1 and 8×1 regular meshes were used.

7.2. Non-linear 2D beam examples

Herein the performance of the proposed non-linear elements based on the ANS method are examined. It should be mentioned that corresponding non-linear elements with or without the ANS interpolation are slightly distinguishable for engineering calculations. Besides, in all tests the tolerance error from relation (43) is set to be $\varepsilon = 10^{-6}$, excepting Section 7.2.1 where $\varepsilon = 10^{-4}$.

7.2.1. Cantilever beam under shear tip load

This problem has been extensively treated for numerical testing of non-linear FE models [5,13]. The cantilever beam has a rectangular cross section, and its mechanical and geometrical characteristics are given in Fig. 6.

Table 3 lists a comparison with the results reported in Refs. [5,13] by using 4×1 nine-node hybrid strain and 8×1 four-node hybrid stress solid-shell elements, respectively, with the numerical Gauss integration scheme. While we used eight two-node curved beam elements with the exact analytical integration. It is seen that both our elements yield a close prediction of the beam response but the TB2S element without the ANS interpolation is a bit stiff. Fig. 7 additionally presents the dependence

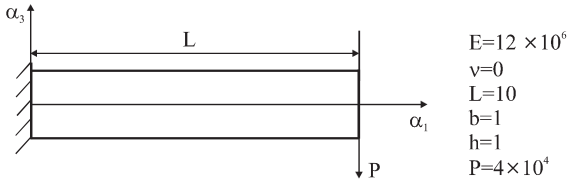

Fig. 6. Cantilever beam under shear tip load.

Table 3
Tip displacements $\bar{v}_i = (v_i^- + v_i^+)/2$ of cantilever beam under shear tip load

Element	Number of steps = 1			Number of steps = 4			Number of steps = 10		
	$-\bar{v}_1$	$-\bar{v}_3$	NIter[a]	$-\bar{v}_1$	$-\bar{v}_3$	NIter[a]	$-\bar{v}_1$	$-\bar{v}_3$	NIter[a]
TB2S	3.350	6.759	8	3.350	6.759	20	3.350	6.759	36
TB2SA	3.404	6.808	8	3.404	6.808	20	3.404	6.806	36
HS (TL) [13]	3.344	6.777	5	3.344	6.777	14	3.344	6.777	30
HS (UL) [13]	3.357	6.785	7	3.357	6.785	17	3.357	6.785	36
Park et al. [5]		6.766	6		6.761	16		6.761	34

[a]NIter denotes a number of iterations.

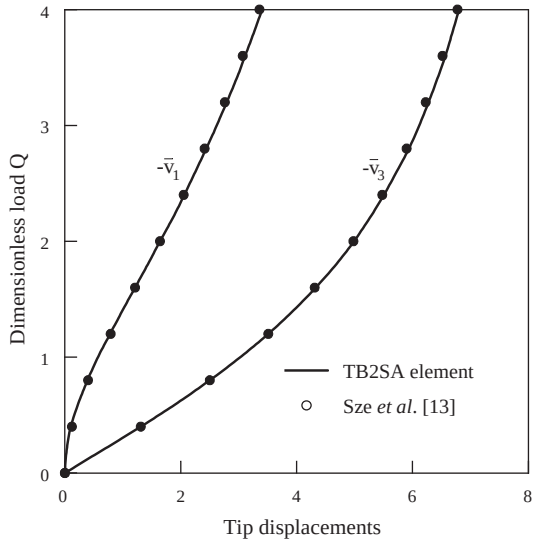

Fig. 7. Longitudinal and transverse tip displacements $\bar{v}_i = \left(v_i^- + v_i^+\right)/2$ of cantilever beam under shear tip load.

of the tip displacements of the centerline on the dimensionless load $Q = PL^2/EI$. The solid lines correspond to all developed two-node hybrid stress–strain ANS elements because Poisson's ratio is equal to zero.

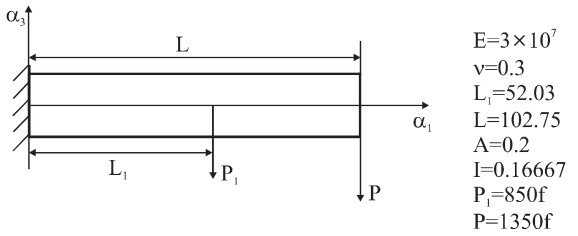

Fig. 8. Cantilever beam under two transverse loads.

Table 4
Tip displacements $\bar{v}_i = (v_i^- + v_i^+)/2$ of cantilever beam under two transverse loads

Loading factor f	Number of nodes	Li [34]		TB2SA		TB2CA		Number of iterations for both elements
		$-\bar{v}_1$	$-\bar{v}_3$	$-\bar{v}_1$	$-\bar{v}_3$	$-\bar{v}_1$	$-\bar{v}_3$	
1	10	—	—	30.87	67.14	28.17	64.67	10
	19	30.78	67.03	30.85	67.08	28.17	64.63	10
	25	30.79	67.02	30.85	67.07	28.17	64.62	10
	49	30.79	67.03	30.85	67.07	28.17	64.61	10
2	49	50.62	80.82	50.73	80.88	48.13	79.42	12
4	49	—	—	67.15	88.62	65.19	87.81	13

7.2.2. *Cantilever beam under two transverse loads*

Consider a cantilever beam subjected to two conservative concentrated loads as shown in Fig. 8, where A is the rectangular cross-section area and I is the inertia moment. This is a typical beam problem with large shearing and has been also used frequently for numerical testing of non-linear finite elements [33–35].

Table 4 lists a comparison with the solution obtained by Li [34] without the thickness change using the four-node Timoshenko beam element in conjunction with five-point Gauss integration scheme. It is seen that all elements perform well but TB2SA and TB2CA elements are less expensive. Note that all our results have been obtained by using *only one* loading step including the last level of loading $f = 4$. In this problem we did not discover an escape of the initial trial value from Newton's attraction area for all reasonable levels of loading. It can be observed that applying the non-uniform meshes improve a solution of this problem. So, the best results are derived for the case $\ell_2/\ell_1 = 2$, where ℓ_1 and ℓ_2 are the lengths of the elements in left and right parts of a beam, respectively. For the complete picture three deformed configurations of this beam are displayed in Fig. 9. One can see that our TB2RA and TB2SA elements are completely free from thickness locking while TB2CA element is too stiff, and its application for the bending dominated beam problems needs great care.

7.2.3. *Deep clamped-hinged arch under apex load*

A deep circular clamped-hinged arch subjected to the conservative concentrated load at the apex (Fig. 10) was first considered by Zienkiewicz using plane stress element and further was studied

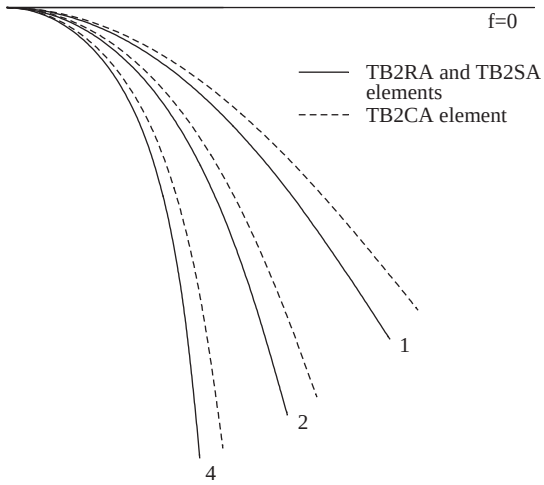

Fig. 9. Deformed configurations of cantilever beam under two transverse loads.

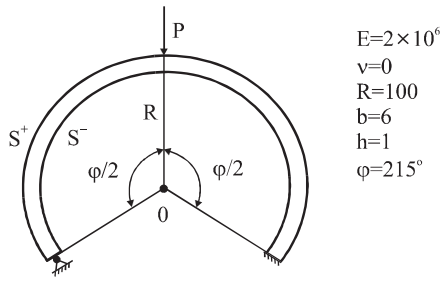

Fig. 10. Deep clamped-hinged arch under apex load.

by many investigators. We did not interest buckling and post-buckling behaviour of the arch. This problem is considered to demonstrate the ability of the present FE formulation to handle finite rotations of curved beams.

Table 5 lists the results reported by Li [34] using 16 four-node Timoshenko beam elements with 5 Gauss integration points and our results obtained by applying 48 TB2SA elements with the full exact analytical integration. The following boundary conditions at the left edge of the arch were used:

$$v_1^- = v_3^- = 0, \tag{44a}$$

$$v_1^+ = v_3^+ = 0, \tag{44b}$$

i.e., either the end point of the bottom line S^- or the end point of the top line S^+ satisfies a physical support condition. One can see that both variants are in a good agreement with Ref. [34] but our results have been obtained by using again *only one* loading step. The number of iterations for each load is listed in Table 5. In addition, Fig. 11 presents four deformed configurations of the arch until snap-through occurs.

Table 5
Displacements $\bar{v}_i = (v_i^- + v_i^+)/2$ of load point of deep clamped-hinged arch

Load PR^2/EI	Li [34]		TB2SA Eq. (44a)		TB2SA Eq. (44b)		Number of iterations
	$-\bar{v}_1$	$-\bar{v}_3$	$-\bar{v}_1$	$-\bar{v}_3$	$-\bar{v}_1$	$-\bar{v}_3$	
2	6.75	8.61	6.84	8.64	6.59	8.44	10
4	21.53	25.70	21.73	25.82	21.17	25.24	16
6	43.11	58.21	43.35	58.60	42.86	57.74	25
8	56.01	93.63	56.40	94.76	55.96	93.74	40

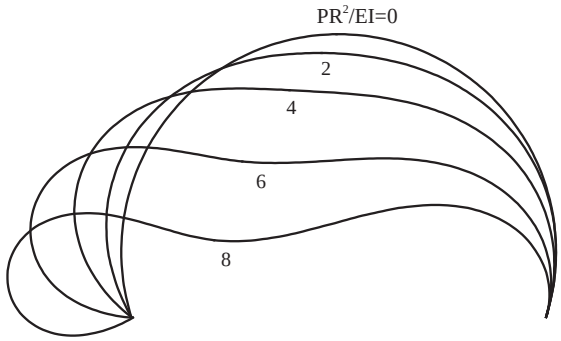

Fig. 11. Deformed configurations of deep clamped-hinged arch under apex load.

7.2.4. Pinched circular sandwich ring

To illustrate more carefully the capability of the developed two-node curved beam elements to overcome thickness locking, we consider a thin circular sandwich ring subjected to two opposite concentrated forces. The geometrical and material properties of the ring are shown in Fig. 12, where R is the radius of the inner circle.

Due to symmetry of the geometry and loading, only one quarter of the ring is modeled with regular meshes of the TB2SA and TB2CA elements. Table 6 lists the convergence results, which are obtained by using *only one* loading step, and a number of iterations for each load. On the order hand, these results illustrate the sensitivity of the TB2CA element to thickness locking. Fig. 13 shows deformed configurations of the inner circle of the ring until a contact of points A and C occurs.

7.3. Non-linear 3D beam examples

The proposed 2D two-node curved beam elements can be readily generalized on the 3D beam elements. For conciseness we investigate only one benchmark problem.

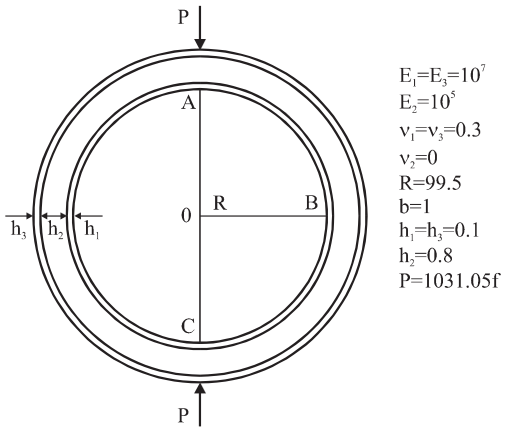

Fig. 12. Pinched circular sandwich ring.

Table 6
Displacements of points A and B of pinched circular sandwich ring

Loading factor f	Number of elements	TB2SA		TB2CA		Number of iterations for both elements
		$-v_3^A$	v_3^B	$-v_3^A$	v_3^B	
1	10	43.87	26.53	38.89	24.65	12
	20	44.61	26.88	39.55	24.98	12
	40	44.80	26.96	39.71	25.06	12
	80	44.85	26.99	39.76	25.08	12
2	10	98.00	33.06	89.43	33.61	17
	20	99.13	33.27	90.60	33.86	16
	40	99.43	33.33	90.91	33.92	16
	80	99.50	33.34	90.99	33.94	16

7.3.1. Cantilever curved beam under tip couple forces

Consider a cantilever curved beam whose centerline is one octant of the circle. The beam is subjected to conservative tip loads in x_3 direction. The geometrical and material data of the problem are given in Fig. 14.

Table 7 lists the results reported in Refs. [33,36–39] using eight straight elements and extracted from the literature in Ref. [40]. Our results have been obtained by modeling a beam with eight TB2SA elements. It should be noted that our results have been found by using *only one* loading step including the last level of loading $Q = 2400$ and 22 iterations were required. And in this problem we did not discover an escape of the initial trial value from Newton's attractive area for all reasonable levels of loading.

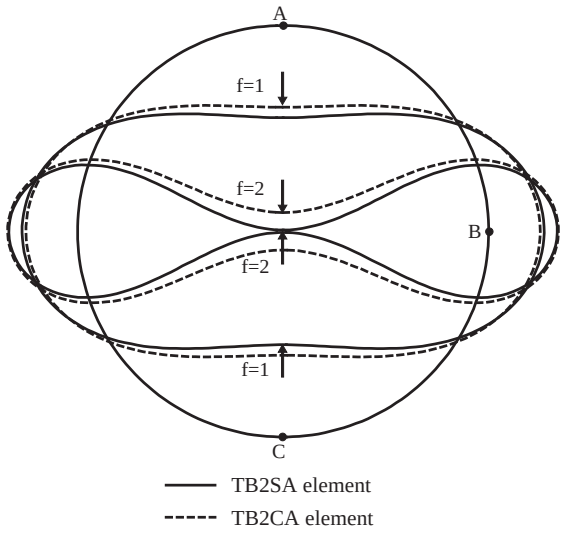

Fig. 13. Deformed configurations of pinched circular sandwich ring.

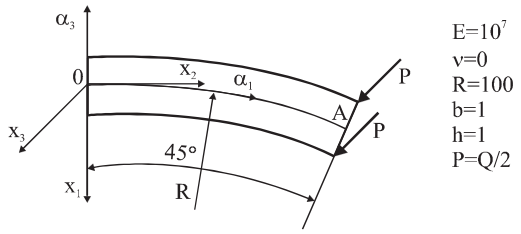

Fig. 14. Cantilever curved beam under tip couple forces.

Table 7
Tip point coordinates of centerline of cantilever curved beam under tip couple forces

Element	$Q = 300$			$Q = 600$			$Q = 2400$		
	x_1^A	x_2^A	x_3^A	x_1^A	x_2^A	x_3^A	x_1^A	x_2^A	x_3^A
Ref. [33]	22.31	58.85	40.08	15.75	47.25	53.37			
Ref. [36]	22.50	59.20	39.50	15.90	47.20	53.40			
Ref. [37]	22.14	58.64	40.35	15.55	47.04	53.50			
Ref. [38]	22.16	58.53	40.53	15.61	47.64	53.71			
Ref. [39]	22.33	58.84	40.08	15.79	47.23	53.37			
Ref. [40]	22.67	58.51	40.14	16.39	46.73	53.33			
TB2SA	22.25	58.79	40.25	15.62	47.03	53.64	5.104	25.23	67.54

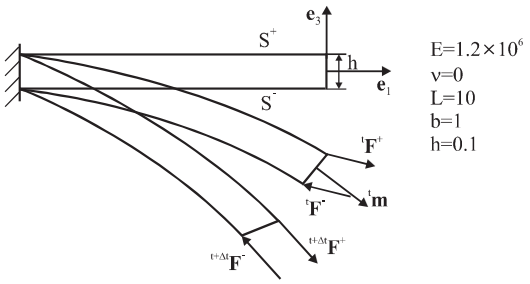

Fig. 15. Deformed configurations of cantilever beam under non-conservative couple forces.

7.4. Non-conservative loading examples

Since the proposed formulation contain no rotational dof, the bending moment cannot be applied directly. Nevertheless, a follower load acting along the beam edge of the current configuration can be accommodated simply [41]. For solving this problem the incremental total Lagrangian formulation [19] will be used.

7.4.1. Cantilever beam under non-conservative couple forces

The cantilever beam subjected to couple forces at the tip (Fig. 15) was selected to study the effect of non-conservative loading. Non-conservative loading is simulated by a pair of opposite forces whose directions are always perpendicular to the current end cross section. During calculations the loading increments are taken to be equal and small in each loading step, to bend a beam into a closed circle. For this purpose the following expressions for the applied incremental forces were used:

$$\Delta\mathbf{F}^{\pm} = {}^{t+\Delta t}\mathbf{F}^{\pm} - {}^{t}\mathbf{F}^{\pm},$$

$${}^{t}\mathbf{F}^{\pm} = \pm {}^{t}P^{t-\Delta t}\mathbf{m}, \quad {}^{t+\Delta t}\mathbf{F}^{\pm} = \pm({}^{t}P + \Delta P)^{t}\mathbf{m},$$

$${}^{t}\mathbf{m} = \frac{1}{\sqrt{1+2{}^{t}\mathscr{E}_{33}}}[(1+{}^{t}\beta_3)\mathbf{e}_1 - {}^{t}\beta_1\mathbf{e}_3], \quad {}^{t}\mathscr{E}_{33} = {}^{t}\beta_3 + \tfrac{1}{2}({}^{t}\beta_1)^2 + \tfrac{1}{2}({}^{t}\beta_3)^2,$$

where ${}^{t}P$ is the loading parameter in the current configuration at time t; ${}^{t}\mathbf{m}$ is the unit vector normal to the end cross section in the current configuration at time t (Fig. 15); ΔP is the loading increment.

The beam is discretized by 20 TB2SA elements. The load is applied in 196 steps of equal magnitude $\Delta P = \pi$. In a result the following accuracy was achieved:

$$|1 + v_1/L| < 10^{-3} \quad \text{and} \quad |v_3/L| < 10^{-3}.$$

The results of the solution of this problem are shown in Figs. 16 and 17. Fig. 17 shows that deformed configurations are circular arcs as predicted by the elasticity theory. An agreement with the analytical solution is good, since an exact value of the bending moment at the tip is $M_{\text{exact}} = 20\pi$. Our FE solution gives $P = 196\pi$, i.e., the applied moment at the tip will be $M = Ph = 19.6\pi$. The better accuracy one can achieve if more increments will be used.

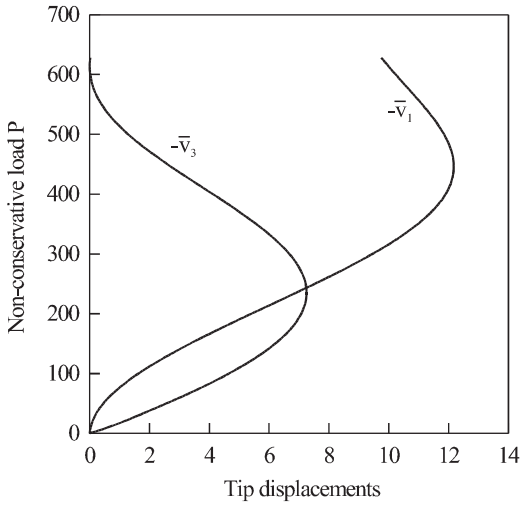

Fig. 16. Longitudinal and transverse tip displacements $\bar{v}_i = (v_i^- + v_i^+)/2$ of cantilever beam under non-conservative couple forces.

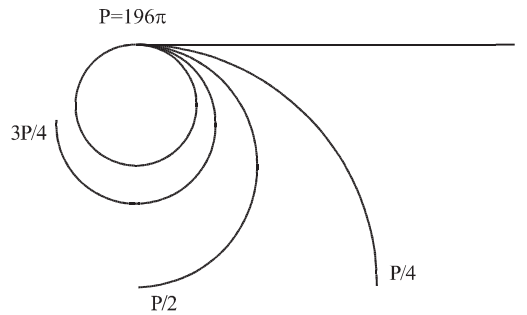

Fig. 17. Deformed configurations of cantilever beam under non-conservative couple forces.

8. Conclusions

The simple and efficient two-node hybrid stress–strain curved beam elements have been developed for the analysis of multilayered Timoshenko beams undergoing finite deformations. The FE formulation is based on the fully non-linear strain–displacement equations that are objective, i.e., invariant under all large rigid-body motions. This is due to our approach in which the displacement vectors of the face lines are introduced and represented in the local reference line basis. So, as fundamental unknowns four displacements of the face lines, and additionally five strains and five conjugate stress resultants have been chosen. This allows in particular special loading conditions at the bottom and top lines, and beam edges to be accounted for.

The proposed refined Timoshenko beam theory is free of assumptions of small displacements, small rotations, small strains and small loading steps because in this paper the exact theory based on the fully non-linear strain–displacement equations has been developed. There exists only one

limitation that a loading step cannot be too large. This restriction arises in the case of using the Newton–Raphson method, since the iteration process can be diverged due to an escape of the trial initial value from Newton's attractive area.

The simplest two-node curved beam elements on the basis of the assumed stress–strain concept have been developed without special stabilization algorithms in a case of the geometrically linear formulation and with ANS interpolation in the *non-linear* case. The governing equations have been obtained by applying the Hu-Washizu variational principle. In a result, the elemental stiffness matrices require only direct substitutions (no inversion is needed) and they can be evaluated using the full exact *analytical* integration. Therefore, our FE formulation is very simple and economical compared to conventional isoparametric formulations. All developed two-node elements do not contain any spurious zero energy modes and possess a proper rank but TB2C and TB2CA elements are too stiff because thickness locking occurs. As concerned a family of TB2R and TB2S elements, they perform excellently.

To demonstrate the high accuracy and efficiency of the developed non-linear FE formulation, several tests for beams under conservative and non-conservative loading were employed. It has been shown that *only one* loading step is needed to obtain the computationally exact solutions of the 2D and 3D beam problems for the extremely large displacements and rotations.

The extension to the finite deformation layer-wise Timoshenko beam theory poses no additional difficulties but requires algebra and computation efforts. This problem is currently under development and will be presented in the next paper.

References

[1] Y.H. Kim, S.W. Lee, A solid element formulation for large deflection analysis of composite shell structures, Comput. Struct. 30 (1988) 269–274.
[2] J.C. Simo, M.S. Rifai, D.D. Fox, On a stress resultant geometrically exact shell model. Part IV. Variable thickness shells with through-the-thickness stretching, Comput. Methods Appl. Mech. Eng. 81 (1990) 91–126.
[3] M. Braun, M. Bischoff, E. Ramm, Nonlinear shell formulations for complete three-dimensional constitutive laws including composites and laminates, Comput. Mech. 15 (1994) 1–18.
[4] H. Parisch, A continuum-based shell theory for non-linear applications, Int. J. Numer. Methods Eng. 38 (1995) 1855–1883.
[5] H.C. Park, C. Cho, S.W. Lee, An efficient assumed strain element model with six dof per node for geometrically nonlinear shells, Int. J. Numer. Methods Eng. 38 (1995) 4101–4122.
[6] P. Betsch, E. Stein, An assumed strain approach avoiding artificial thickness straining for a nonlinear 4-node shell element, Commun. Numer. Methods Eng. 11 (1995) 899–909.
[7] P. Betsch, F. Gruttmann, E. Stein, A 4-node finite shell element for the implementation of general hyperelastic 3D-elasticity at finite strains, Comput. Methods Appl. Mech. Eng. 130 (1996) 57–79.
[8] R. Hauptmann, K. Schweizerhof, A systematic development of 'solid-shell' element formulations for linear and non-linear analyses employing only displacement degrees of freedom, Int. J. Numer. Methods Eng. 42 (1998) 49–69.
[9] B.L. Kemp, C. Cho, S.W. Lee, A four-node solid shell element formulation with assumed strain, Int. J. Numer. Methods Eng. 43 (1998) 909–924.
[10] S. Klinkel, F. Gruttmann, W. Wagner, A continuum based three-dimensional shell element for laminated structures, Comput. Struct. 71 (1999) 43–62.
[11] C. Sansour, F.G. Kollmann, Families of 4-node and 9-node finite elements for a finite deformation shell theory. An assessment of hybrid stress, hybrid strain and enhanced strain elements, Comput. Mech. 24 (2000) 435–447.
[12] K.Y. Sze, S.H. Lo, L.Q. Yao, Hybrid-stress solid elements for shell structures based upon a modified variational functional, Int. J. Numer. Methods Eng. 53 (2002) 2617–2642.

[13] K.Y. Sze, W.K. Chan, T.H.H. Pian, An eight-node hybrid-stress solid-shell element for geometric non-linear analysis of elastic shells, Int. J. Numer. Methods Eng. 55 (2002) 853–878.
[14] S. Ahmad, B.M. Irons, O.C. Zienkiewicz, Analysis of thick and thin shell structures by curved shell elements, Int. J. Numer. Methods Eng. 2 (1970) 419–451.
[15] K.Y. Sze, Three-dimensional continuum finite element models for plate/shell analysis, Prog. Struct. Eng. Mater. 4 (2002) 400–407.
[16] G.M. Kulikov, S.V. Plotnikova, Comparative analysis of two algorithms for numerical solution of nonlinear static problems for multilayered anisotropic shells of revolution. 2. Account of transverse compression, Mech. Compos. Mater. 35 (1999) 293–300.
[17] G.M. Kulikov, S.V. Plotnikova, Finite element formulation of straight composite beams undergoing finite rotations, Trans. Tambov State Tech. Univ. 7 (2001) 617–633.
[18] G.M. Kulikov, S.V. Plotnikova, Investigation of locally loaded multilayered shells by a mixed finite-element method. 2. Geometrically nonlinear statement, Mech. Compos. Mater. 38 (2002) 539–546.
[19] G.M. Kulikov, S.V. Plotnikova, Non-linear strain-displacement equations exactly representing large rigid-body motions. Part I. Timoshenko-Mindlin shell theory, Comput. Methods Appl. Mech. Eng. 192 (2003) 851–875.
[20] G.M. Kulikov, S.V. Plotnikova, Finite deformation plate theory and large rigid-body motions, Int. J. Non-Linear Mech. 39 (2004) 1093–1109.
[21] G. Wempner, D. Talaslidis, C.M. Hwang, A simple and efficient approximation of shells via finite quadrilateral elements, J. Appl. Mech. 49 (1982) 115–120.
[22] K.Y. Sze, S. Yi, M.H. Tay, An explicit hybrid stabilized eighteen-node solid element for thin shell analysis, Int. J. Numer. Methods Eng. 40 (1997) 1839–1856.
[23] G.M. Kulikov, Analysis of initially stressed multilayered shells, Int. J. Solids Struct. 38 (2001) 4535–4555.
[24] G.M. Kulikov, Non-linear analysis of multilayered shells under initial stress, Int. J. Non-Linear Mech. 36 (2001) 323–334.
[25] E.I. Grigolyuk, G.M. Kulikov, Multilayered Reinforced Shells: Analysis of Pneumatic Tires, Mashinostroyenie, Moscow, 1988 (in Russian).
[26] K. Washizu, Variational Methods in Elasticity and Plasticity, Pergamon Press, Oxford, 1982.
[27] G.M. Kulikov, S.V. Plotnikova, Simple and effective elements based upon Timoshenko-Mindlin shell theory, Comput. Methods Appl. Mech. Eng. 191 (2002) 1173–1187.
[28] T.J.R. Hughes, T.E. Tezduyar, Finite elements based upon Mindlin plate theory with particular reference to the four-node bilinear isoparametric element, J. Appl. Mech. 48 (1981) 587–596.
[29] R.H. MacNeal, Derivation of element stiffness matrices by assumed strain distributions, Nucl. Eng. Design 70 (1982) 3–12.
[30] K.J. Bathe, E.N. Dvorkin, A formulation of general shell elements—the use of mixed interpolation of tensorial components, Int. J. Numer. Methods Eng. 22 (1986) 697–722.
[31] S.W. Lee, T.H.H. Pian, Improvement of plate and shell finite element by mixed formulations, AIAA J. 16 (1978) 29–34.
[32] C. Cho, S.W. Lee, On the assumed strain formulation for geometrically nonlinear analysis, Finite Elements Anal. Design 24 (1996) 31–47.
[33] L.A. Crivelli, et al., A three-dimensional non-linear Timoshenko beam based on the core-congruental formulation, Int. J. Numer. Methods Eng. 36 (1993) 3647–3673.
[34] M. Li, The finite deformation theory for beam, plate and shell. Part I. The two-dimensional beam theory, Comput. Methods Appl. Mech. Eng. 146 (1997) 53–63.
[35] M. Li, F. Zhan, The finite deformation theory for beam, plate and shell. Part IV. The FE formulation of Mindlin plate and shell based on Green-Lagrangian strain, Comput. Methods Appl. Mech. Eng. 182 (2000) 187–203.
[36] K.J. Bathe, S. Bolourchi, Large displacement analysis of three-dimensional beam structures, Int. J. Numer. Methods Eng. 14 (1979) 961–986.
[37] A. Cardona, M. Geradin, A beam finite element non-linear theory with finite rotation, Int. J. Numer. Methods Eng. 26 (1988) 2403–2438.
[38] M.A. Crisfield, A consistent co-rotational formulation for non-linear three-dimensional beam elements, Comput. Methods Appl. Mech. Eng. 81 (1990) 131–150.

[39] J.C. Simo, L. Vu-Quoc, A three-dimensional finite strain rod model. Part II. Computational aspects, Comput. Methods Appl. Mech. Eng. 58 (1986) 79–116.
[40] M. Li, The finite deformation theory for beam, plate and shell. Part III. The three-dimensional beam theory and the FE formulation, Comput. Methods Appl. Mech. Eng. 162 (1998) 287–300.
[41] G. Horrigmoe, P.G. Bergan, Nonlinear analysis of free-form shells by flat finite elements, Comput. Methods Appl. Mech. Eng. 16 (1978) 11–35.